

# Observable $\phi_\eta^*$ at LHC and second-order QED matrix element in $Z/\gamma^* \rightarrow l^+l^-$ decays

Thi Kieu Oanh Doan<sup>a</sup>, W. Płaczek<sup>b</sup> and Z. Wąs<sup>c,d</sup>

<sup>a</sup>*LAPP Annecy, CNRS, France.*

<sup>b</sup>*Marian Smoluchowski Institute of Physics, Jagiellonian University,  
ul. Reymonta 4, 30-059 Krakow, Poland.*

<sup>c</sup>*Institute of Nuclear Physics, PAN, ul. Radzikowskiego 152, Krakow, Poland.*

<sup>d</sup>*CERN PH-TH, CH-1211 Geneva 23, Switzerland.*

## Abstract

In a recent publication by ATLAS collaboration a new observable, the so-called  $\phi_\eta^*$  angle, was used for precise measurement of transverse  $Z$  momentum. One of the dominant systematic errors for this measurement originates from the theoretical control of QED final-state bremsstrahlung. At present, it is estimated at the 0.3% level for the shape of the  $\phi_\eta^*$  distribution. In this paper we discuss the possible effects of the second-order QED matrix element for that quantity. For that purpose, results from simulations based on the Yennie–Frautchi–Suura (YFS) exponentiation and featuring the second-order matrix elements are used and compared with the case when the matrix element is restricted to the first order. From this study we conclude that in order to reach the precision below 0.3% for the  $\phi_\eta^*$  distribution at the LHC, inclusion of the second-order QED matrix element in a respective Monte Carlo event generator is necessary.

# 1 Introduction

The main purpose of LHC experiments is to search for new elementary particles and interactions. The Higgs-like particle observability papers [1, 2] document a fundamental achievement for this goal. Another important class of the LHC measurements aims on high-precision consistency tests of the Standard Model. In this respect, a precise measurement of the  $W$  mass plays a particularly important role [3]. To reduce systematic errors, improvements in the measurement techniques are desirable. It is generally believed that higher precision can be achieved thanks to the use, whenever possible, of leptonic degrees of freedom rather than hadronic ones. In this way the precision better by even an order of magnitude can be achieved. At present, the best measurements of  $W$  mass have been performed in  $p\bar{p}$  collisions at Tevatron [4, 5, 6]. In the CDF collaboration the precision of 19 MeV on the  $W$  mass was achieved. They have estimated that the largest contribution from theory to the systematic error originates from parton distribution functions (PDF's) and initial-state hadronic interactions in general.

An approach [7, 8, 9] based on measuring the  $\phi_\eta^*$  angle, instead of  $Z$  transverse momentum ( $p_T^Z$ ), may offer a significant improvement. In Ref. [10] the first results of  $\phi_\eta^*$  measurements with ATLAS experiment were presented already. In that experimental publication the systematic error of 0.3% to  $\phi_\eta^*$  due to implementation of QED final state radiation (FSR) in the Monte Carlo generators used, was estimated in proportion of differences observed between PHOTOS [11, 12, 13] and SHERPA [14] predictions. If one understands the pattern of these differences, one can hopefully reduce systematic errors further. In this sense presented here work is continuation of recent efforts in this direction documented in Ref. [15].

One of the possible sources of the above differences may be the second-order matrix element for QED final-state radiation (FSR) in  $Z$  decays. Such a matrix element is missing in PHOTOS and in SHERPA, but its dominant contribution is taken into account thanks to iterative and/or multiphoton nature of the algorithms. Multitude of tests for PHOTOS were devoted to this point over time [12, 15, 16]. In particular, it was shown [11] that despite the fact that PHOTOS is not using a matrix-element-based kernel, it agrees substantially better with distributions obtained from the KKMC Monte Carlo [17] if exclusive exponentiation featuring the second-order matrix element is used rather than if the matrix element is restricted to the first-order only. The KKMC program is particularly suitable as a source of precise numerical benchmarks, because its precision was studied at the LEP time in a great detail, see e.g. Ref. [18], and with precision requirements surpassing the present-day requirements of the LHC experiments. It is known since more than 20 years now [19] that second-order terms are necessary for an exponentiation-based Monte Carlo generator if it is expected to assure a high precision in the case of precision observables of  $e^+e^-$  colliders. That is why such terms were implemented in the  $e^+e^- \rightarrow l^+l^-$  generators KORALZ [20] and in the KKMC program as well. The precision of 0.06% was evaluated in [21] for small-angle Bhabha scattering simulated with the Monte Carlo generator BHLUMI [22].

For the LHC applications, the second-order QED FSR matrix element was found to be important for simulations of background for Higgs-boson searches in the  $2\gamma$  channel

[16]. With time and improving experimental precision, contribution from the second-order QED FSR matrix element may become important for more inclusive observables at the LHC as well. First attempts to implement the second-order matrix element (ME) to the LHC Monte Carlo generators are on-going; a good example is [23].

Before such projects are completed, let us provide some quantitative results using the LEP-era Monte Carlo program *KKMC*. For emulation of the initial-state hadronic interactions, parton distribution functions (PDF's) combined with the transverse momentum smearing based on the *RESBOS* program [24] are used only. Such an approach doesn't take into account the detector simulations, nonetheless it should be sufficient to quantify the size of the effect of the second-order ME.

Our note is organized as follows. In Section 2 we describe our Monte Carlo set-up. Section 3 is devoted to a careful definition of the  $\phi_\eta^*$  distribution, including selections criteria, etc. In Section 4 we present our numerical results. Section 5 summarizes the paper with conclusions.

## 2 Monte Carlo set-up

The *KKMC* event generator is constructed for  $e^+e^- \rightarrow \mu^+\mu^-(\tau^+\tau^-, q\bar{q})$  processes and for centre-of-mass system energies from the production threshold up to 200 GeV. For our purposes it was adapted to work for quark-anti-quark annihilation process  $q\bar{q} \rightarrow l^+l^-$ . However, in this case, only QED FSR can be generated. By default, the second-order matrix element is active, but the program can be downgraded to the first-order FSR as well. We use this program as a building block in our simulation chain. With the help of *WINHAC*, the MC event generator for Drell–Yan processes [25, 26], using the *MSTW2008NLO* [27] parametrisation of PDF's we generate a series of the Bjorken variables  $x_1$  and  $x_2$  for  $pp$  collisions at  $\sqrt{s} = 7$  TeV corresponding to production of  $Z$ -bosons in a very narrow invariant mass range:  $M_Z \pm 1$  MeV. Then we generate monochromatic  $Z$  decays including QED FSR bremsstrahlung. Let us stress that we aim at the estimation of a small second-order QED FSR effect and not at the complete predictions. That is why we can limit ourselves to the dominant QCD initial-state effects only.

The generated sample has to be convoluted with the initial-state QCD effects. For the sake of convolution, each generated  $q\bar{q} \rightarrow Z \rightarrow e^+e^-n(\gamma)$  event is boosted to the laboratory frame using  $x_1$  and  $x_2$  of the incoming quarks generated by *WINHAC* Monte Carlo [25, 26]. To emulate transverse momentum of  $Z$  we use smearing on the basis of a  $p_T^Z$  distribution (histogram) obtained from the *RESBOS* program [24], which was found to model data within the 4% accuracy, as concluded in Ref. [10]. From this distribution we randomly generate  $p_T^Z$  of the  $Z$  boson, to be used in the boost to the laboratory frame. This is a crude approximation which, again, is acceptable in evaluation of the considered effect, only because it is expected to be small. In Fig. 1, distributions of  $p_T^Z$  and  $y_Z$  (for  $u\bar{u}$  annihilation) are reproduced for the reference.

Two versions of the results will be compared: the one when the exclusive exponentiation, as embedded in *KKMC*, is featuring the second-order matrix element (option *CEEX2*)

and the another one when it is limited to the first-order only (option CEEEX1), as defined in Ref. [18]. The technical advantage of correlated samples will help to control differences for the two options in less populated regions of the phase space. The CEEEX1 variant will be implemented with an appropriate weight. This is advantageous, as we expect the difference of CEEEX2 and CEEEX1 to be rather small, but at the same time limitations due to restricted treatment of the initial-state hadronic interactions are present. We have to limit ourselves (for the particular run) to a fixed flavour of quarks entering the hard process, moreover the virtuality of the intermediate state has to be fixed as well. For the presented plots the incoming  $u$ -quarks were chosen and the intermediate-state virtuality was fixed in KKMC generation to  $Z$  boson mass. The results for the incoming  $d$ -quarks essentially coincide with the presented ones.

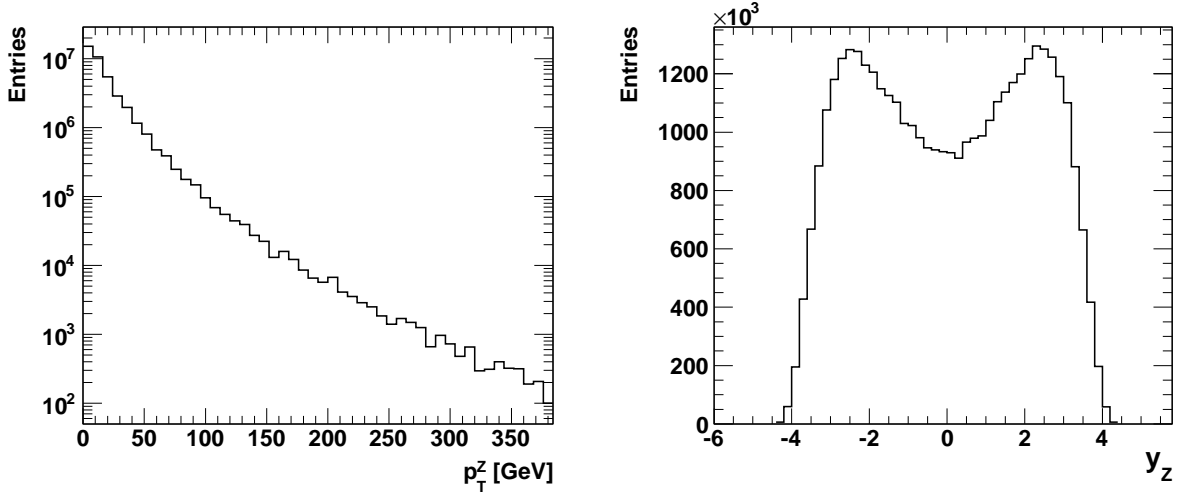


Figure 1: The distributions of the  $Z$  transverse momentum  $p_T^Z$  (left) and rapidity  $y_Z$  (right) constructed from the Monte Carlo sample used in our study. No selection cuts were applied. The quark-level hard process of  $u\bar{u}$  annihilation at the center-of-mass energy equal to 91.187 GeV of  $pp$  collisions at 7 TeV was used. Note minor imperfections, due to only a discrete set of values generated for the  $p_T^Z$  distribution; they are present also in Fig. 3.

### 3 Definition of observable $\phi_\eta^*$

As proposed and studied in Refs. [7, 8, 9], an alternative observable to study the  $Z$  transverse momentum ( $p_T^Z$ ) is  $\phi_\eta^*$ , defined [8] as:

$$\phi_\eta^* \equiv \tan \frac{\phi_{\text{acop}}}{2} \sin \theta_\eta^*, \quad (1)$$

where  $\phi_{\text{acop}} \equiv \pi - \Delta\phi$ ,  $\Delta\phi$  is the azimuthal opening angle between the two leptons, and the angle  $\theta_\eta^*$  is a measure of the scattering angle of the leptons with respect to the proton

beam direction in the rest frame of the dilepton system. The angle  $\theta_\eta^*$  is defined [8] by  $\cos \theta_\eta^* \equiv \tanh[(\eta^- - \eta^+)/2]$ , where  $\eta^-$  and  $\eta^+$  are the pseudorapidities of the negatively and positively charged lepton, respectively.

The observable  $\phi_\eta^*$  is expected to be less sensitive to experimental resolution and it can probe largely the same physics as  $p_T^Z$  for small  $p_T^Z$  or  $\phi_\eta^*$ . The theoretical calculations for the  $\phi_\eta^*$  are documented in Refs. [28, 29]. The first experimental measurement of the  $\phi_\eta^*$  by the D0 Collaboration [30] demonstrated that the order of magnitude improvements in experimental precision could be achieved with the  $\phi_\eta^*$  technique. The  $\phi_\eta^*$  was then employed by the ATLAS and LHCb experiments in recent publications [10, 31]. The first measurement of the normalized  $\phi_\eta^*$  distribution at  $\sqrt{s} = 7$  TeV  $pp$  collisions performed by the ATLAS experiment is very likely one of the most precise measurement at the LHC, with the total uncertainty at the level of 0.5–0.8%. The normalized differential cross section was defined [10] as  $1/\sigma^{\text{fid}} \cdot d\sigma^{\text{fid}}/d\phi_\eta^*$ , where  $\sigma_{\text{fid}}$  is measured within the fiducial lepton acceptance defined by the lepton ( $\ell = e, \mu$ ) transverse momentum  $p_T^\ell > 20$  GeV, the lepton pseudorapidity  $|\eta^\ell| < 2.4$  and the invariant mass of the lepton pair:  $66 \text{ GeV} < m_{\ell\ell} < 116 \text{ GeV}$ . In [10] three lepton definitions with respect to the QED FSR were used. A "bare" level defined directly by the final-state leptons after QED FSR will be followed in our paper. A "dressed" level is defined if lepton four-momenta are recombined with photons radiated within a cone of  $\Delta R = \sqrt{(\Delta\eta)^2 + (\Delta\phi)^2} = 0.1$ . Finally, a "Born" level is defined when four-momenta of the final-state leptons before Monte Carlo simulation of QED FSR are used. The measured  $\phi_\eta^*$  distribution in data after correcting only for all detector effects is at bare level. To account for QED FSR effects and to obtain the  $\phi_\eta^*$  distribution at Born and dressed level a correction, computed using PHOTOS was applied to the data.

The dominant systematic uncertainty of this measurement is due to  $\phi_\eta^*$ -dependent modelling of QED FSR in this correction, assigned to be 0.3% by comparing predictions from PHOTOS (interfaced in POWHEG+PYTHIA6) [32, 33] and SHERPA, as studied in Ref. [34]. This uncertainty is extracted by looking at the ratio between the normalized  $\phi_\eta^*$  distribution predictions at the dressed or bare levels and the one at the Born level in PHOTOS and in SHERPA.

The uncertainties on this correction are extracted by looking at the ratio between the normalized  $\phi_\eta^*$  distribution at the dressed or bare levels and the one at the Born level in PHOTOS and in SHERPA (in all cases no detector smearing effects are introduced).

The ratio of the predictions of PHOTOS and SHERPA in the case of the electron channel is shown<sup>1</sup> in Fig. 6.5 of Ref. [34]. Statistical fluctuations are too large to draw firm conclusions, nevertheless a hint of difference (wavy structure) seems present which appear to be more profound when comparing the two programs for the bare case. One can only partly profit from the statistical correlation of the left and right hand side plots of Fig. 6.5 which are constructed from the same sample of events.

We can investigate this difference by means of comparing the results from KKMC: at the first-order mode and at the second order mode. This comparison is expected to be sensitive

---

<sup>1</sup>Fig. 6.5 of Ref. [34] is available on-line from [this hyperlink](#).

to a pure QED effect. The difference as a function of  $\phi_\eta^*$  can be used as an correction or as estimation of the systematic error for the missing second-order matrix element of QED. We present details of the comparison in the following section.

## 4 Numerical results

We combine histograms and plot superimposed distributions for  $\phi_\eta^*$  in the case when the first and second-order QED FSR matrix elements are used in **KKMC**. **KKMC** is not suitable for simulations of events in  $pp$  collisions. We overcome this obstacle by switching off all the QED initial-state radiation in **KKMC**, the final-state radiation is then retained only. We replace the incoming electrons with quarks. Generation of  $q\bar{q} \rightarrow l^+l^-n\gamma$  events at the fixed centre-of-mass energy can be then performed. We use several fixed quark-pair virtualities close to the  $Z$  peak<sup>2</sup>.

For the **KKMC**-based plots the following cuts were used. These cuts are similar but not identical with the one used in experimental studies described earlier. We request  $p_T^{l^\pm} > 20$  GeV,  $|\eta_{l^\pm}| < 2.4$ , in our case the region  $1.37 < |\eta_{l^\pm}| < 1.52$  was rejected. Finally, acoplanarity for leptons was requested to be smaller than 3. We have used bare electrons only. We have investigated several options for the cut on lepton pair mass  $m_{ee}$  and not only the default one used by the ATLAS experiment:  $66 \text{ GeV} < m_{ee} < 116 \text{ GeV}$ . The cut removes hard-photon configurations and reduces higher-order QED effects, as can be seen in Fig. 3: from 0.2–0.3% to below 0.1%. The sample used for construction of these plots was with the  $Z$  virtuality equal to  $M_Z$ , but we have checked the contributions from higher virtualities of an intermediate state as well. Then, see Fig. 3, the correction was higher, even if the  $m_{ee}$  cut was present – it approached 2%.

In Fig. 2 we show the results with realistic cuts for  $\phi_\eta^*$  defined in the previous section, where the effects of the longitudinal momentum of  $Z$  due to PDF's are taken into account. The transverse momentum,  $p_T^Z$ , of  $Z$  is, however, set to zero. As a consequence,  $\phi_\eta^*$  is non-zero only because of QED FSR. At least one photon is needed for events to populate other bins than the first one. That is why the effects of the second-order ME corrections are numerically large. They represent leading correction: nearly all events are placed in the first bin of the histogram, corresponding to  $\phi_\eta^* = 0$  or below the detector resolution, whereas contents of all other bins are at least two order of magnitude smaller. The second-order matrix element represent the correction which grows from 1% to 15% at the end of the spectrum. As expected, the **CEEX1** prediction is larger for large  $\phi_\eta^*$ . The  $\beta_1$  correction of the YFS exponentiation is negative for hard photons [18].

For Fig. 3 no restrictions on  $p_T^Z$  spectrum were introduced and one can see that the correction is small over the whole range of  $\phi_\eta^*$ , nonetheless grows up to 0.2% at the end of the spectrum. This is consistent with what we observe in Fig. 6.5 of Ref. [34] at the end

---

<sup>2</sup> Before collecting numerical results, we have checked that our calculation for observable  $\phi_\eta^*$  is properly defined. We have coded independently the  $\phi_\eta^*$  angle and the event selection criteria in the **FORTAN** and **C++** programming languages.



of the spectrum for bare leptons. The distributions of the  $Z$  transverse momentum  $p_T^Z$  and its rapidity  $y_Z$  without any cuts, used in our MC simulations, are shown in Fig. 1.

It is technically simple to prepare such kind of plots for the comparisons of PHOTOS and KKMC, but similar results have recently been presented in Ref. [15]. Also the comparisons with other variants of the matrix element implementation in KKMC, such as EEX1, EEX2, EEX3, may be instructive for detailed study aiming at the precision implementation of the exclusive exponentiation algorithms into  $pp$  collisions Monte Carlo generators. This is, however, out of the scope of this work.

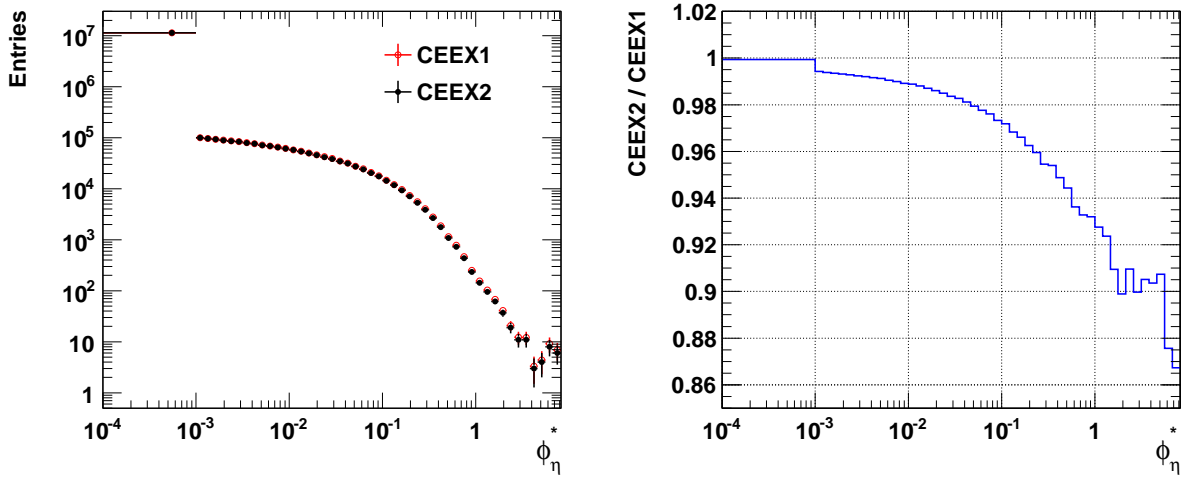


Figure 2: The  $\phi_\eta^*$  distribution: the comparisons of the CEEEX2 and CEEEX1 results. The sample of  $u\bar{u} \rightarrow e^+e^-(n\gamma)$  events is generated. The virtuality of the  $Z$  boson equal to its mass is used. The boost to the laboratory frame of  $Z$  is performed prior to histogramming with cuts. The longitudinal momentum of  $Z$  is generated according to WINHAC in  $pp$  collision at  $\sqrt{s} = 7$  TeV, while  $p_T^Z = 0$ . In the first bin, the configurations with  $\phi_\eta^*$  smaller than 0.001 are collected.

Let us now comment on the reliability of presented results. In left hand-side plot of Fig. 6.5 from Ref. [34], the corrections for the  $\phi_\eta^*$  calculated with dressed electrons, are compared for the SHERPA and PHOTOS cases; they coincide down to about 0.1%. The distinct treatment of hadronic initial-state interactions in PYTHIA and SHERPA can not therefore be the prime source of the wavy structure in  $\phi_\eta^*$  corrections calculated for the similar plot but with bare electrons, see right-hand side of Fig. 6.5. Note that the two plots of Fig. 6.5 are in part statistically correlated as they are constructed from the same sample of events.

The difference between dressed and bare cases likely originates from the different treatment of collinear photons. We may deduce from Fig. 6.5 and our Fig. 3 that absent in SHERPA second-order QED FSR matrix element can in part be responsible for the observed hint of the difference in corrections calculated for bare electrons with the two programs. In PHOTOS second-, and higher-order QED FSR terms, important in collinear limits, are taken into account thanks to iterative algorithm.

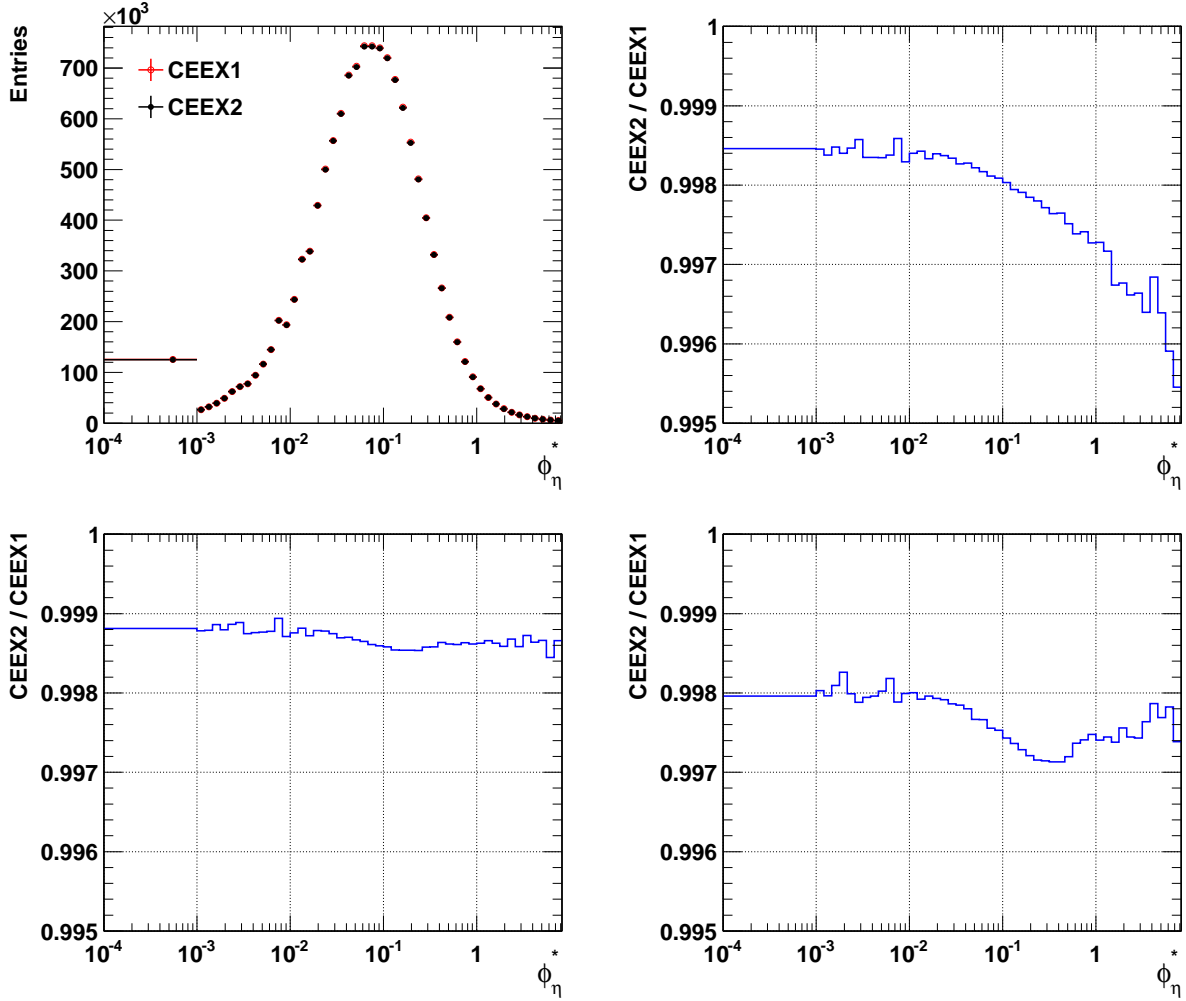


Figure 3: The  $\phi_\eta^*$  distribution: the comparisons of the CEEX2 and CEEX1 results. The sample of  $u\bar{u} \rightarrow e^+e^-(n\gamma)$  events is generated. The virtuality of the  $Z$  boson equal to its mass is used. The longitudinal momentum of  $Z$  is generated according to WINHAC in  $pp$  collision at  $\sqrt{s} = 7$  TeV, while its transverse momentum is generated according to the prescription given in the text. The boost to the laboratory frame of  $Z$  is performed prior to histogramming with cuts. In the first bin, the configurations with  $\phi_\eta^*$  smaller than 0.001 are collected. In the upper row of plots, cuts as explained in the text except cut on  $m_{ee}$ , are used. The plot with  $66 \text{ GeV} < m_{ee} < 116 \text{ GeV}$  is on the bottom-left side. On the bottom-right side, where in addition to this cut, exceptionally the events with the  $Z/\gamma^*$  virtuality of 115 GeV are taken, a wavy structure of the correction appears. For the virtuality above 116 GeV the correction becomes larger, 2% or more, because the no-bremsstrahlung events do not contribute. This demonstrates the limitations of our approach. Contributions from all  $Z/\gamma^*$  virtualities have to be combined for realistic prediction, rather than of fixed ones, we have used for the estimate of the effect size.



## 5 Summary

In this paper we have studied the effect of the second-order matrix element with respect to the first-order one. We have concentrated mainly on the case when bare electrons were used, because it was contributing to the discussion of the systematic error in measurement of Ref. [10]. The Monte Carlo simulation based on the exponentiation was used for the QED final-state radiation. The  $\phi_\eta^*$  distribution in  $Z/\gamma \rightarrow e^+e^-n(\gamma)$  production and decay at LHC was studied. We have started with the case when  $p_T$  of the decaying  $Z$  was set to zero, see Fig. 2, the effect of the introduction of the second-order matrix element was large, at the level of 1–15%. However, the bulk of the distribution resided in the first bin of the histogram of  $\phi_\eta^* < 0.001$ .

When the initial-state  $Z$ -boson  $p_T^Z$  is taken into account, then the  $\phi_\eta^*$  distribution is representing convolution of the dominant effect of initial-state quark transverse momenta and the QED FSR correction. The effect of  $p_T^Z$  of the incoming  $Z$  dominates. The corrections due to the second order matrix element are smaller in the case of dressed leptons. This is consistent if the effect is due to consecutive collinear photons. Already the second-hardest photon requires the **CEEX2** matrix element to be present in the exponentiation-based MC simulations. The ratio of the parameters defining the range of the lepton-pair invariant mass  $m_{ll}$  to the virtuality of the intermediate  $Z/\gamma^*$  used in our generation seems to be decisive for the details of the shape of the **CEEX2-CEEX1** differences.

We can conclude that starting from the precision better than 0.3% for the  $\phi_\eta^*$  distribution, the dominant contribution of the second-order QED FSR matrix element has to be included in discussion of systematic errors for Monte Carlo simulations used for the LHC experiments.

The above effects are slightly larger than presently aimed precision for the fermion-pair emission or interference, as discussed in Ref. [15] for example. The  $\phi_\eta^*$  is an example of relatively inclusive observable, where at the least, dominant parts of the second-order QED FSR effects have to be taken into account, even if the exclusive exponentiation is in use.

We could observe that the effect of the second-order matrix element was more significant in the case of the  $\phi_\eta^*$  observable defined with the bare leptons than with the dressed ones, again confirming that the dominant effect is of the leading-logarithmic nature. That is why, one may expect that for many applications, the systematic error concluded in Ref. [10] is an overestimation. To understand when it is actually the case, more detailed studies of cut-off dependence than presented in this paper are necessary.

## Acknowledgements

Part of this work has been inspired by the discussion with Lucia di Ciaccio, Elzbieta Richter-Was, Stanislaw Jadach and members of the ATLAS LAPP-Annecy group; continuous encouragement and comments on intermediate steps of the work are acknowledged. The work is supported in part by the Polish National Centre of Science Grants No. DEC-2011/03/B/ST2/00220 and DEC-2012/04/M/ST2/00240, and by the Programme of the

French–Polish Co-operation between IN2P3 and COPIN within the Collaborations Nos. 10-138 and 11-142.

## References

- [1] ATLAS Collaboration Collaboration, G. Aad *et al.*, *Phys. Lett.* **B716** (2012) 1–29, 1207.7214.
- [2] CMS Collaboration Collaboration, S. Chatrchyan *et al.*, *Phys. Lett.* **B716** (2012) 30–61, 1207.7235.
- [3] ATLAS Collaboration, N. Besson, M. Boonekamp, E. Klinkby, and T. Petersen, ATL-COM-PHYS-2009-102, ATL-PHYS-PUB-2009-036.
- [4] CDF Collaboration, T. Aaltonen *et al.*, *Phys. Rev. Lett.* **104** (2010) 201801, 0912.4500.
- [5] CDF Collaboration, T. Aaltonen *et al.*, *Phys. Rev. Lett.* **108** (2012) 151803, 1203.0275.
- [6] D0 Collaboration, V. M. Abazov *et al.*, *Phys. Rev. Lett.* **108** (2012) 151804, 1203.0293.
- [7] M. Vesterinen and T. Wyatt, *Nucl. Instrum. Meth.* **A602** (2009) 432, 0807.4956.
- [8] A. Banfi, S. Redford, M. Vesterinen, P. Waller, and T. Wyatt, *Eur. Phys. J.* **C71** (2011) 1600, 1009.1580.
- [9] A. Banfi, M. Dasgupta, and S. Marzani, *Phys. Lett.* **B701** (2011) 75, 1102.3594.
- [10] ATLAS Collaboration, G. Aad *et al.*, *submitted to Phys. Lett. B* (2012) 1211.6899.
- [11] P. Golonka and Z. Was, *Eur. Phys. J.* **C45** (2006) 97–107, hep-ph/0506026.
- [12] P. Golonka and Z. Was, *Eur. Phys. J.* **C50** (2007) 53–62, hep-ph/0604232.
- [13] E. Barberio and Z. Was, *Comput. Phys. Commun.* **79** (1994) 291–308.
- [14] T. Gleisberg, S. Hoeche, F. Krauss, M. Schonherr, S. Schumann, *et al.*, *JHEP* **0902** (2009) 007, 0811.4622.
- [15] A. Arbuzov, R. Sadykov, and Z. Was, 1212.6783.
- [16] E. Richter-Was, *Z. Phys.* **C61** (1994) 323.
- [17] S. Jadach, Z. Was, and B. F. L. Ward, *Comput. Phys. Commun.* **130** (2000) 260, Up to date source available from <http://home.cern.ch/jadach/>.

- [18] S. Jadach, B. Ward, and Z. Was, *Phys. Rev.* **D63** (2001) 113009, [hep-ph/0006359](#).
- [19] S. Jadach and B. F. L. Ward, *Phys. Lett.* **B274** (1992) 470–472.
- [20] S. Jadach, B. F. L. Ward, and Z. Was, *Comput. Phys. Commun.* **79** (1994) 503.
- [21] B. Ward, S. Jadach, M. Melles, and S. Yost, *Phys. Lett.* **B450** (1999) 262–266, [hep-ph/9811245](#).
- [22] S. Jadach, W. Placzek, E. Richter-Was, B. Ward, and Z. Was, *Comput. Phys. Commun.* **102** (1997) 229–251.
- [23] S. Yost, V. Halyo, M. Hejna, and B. Ward, [1201.5906](#).
- [24] C. Balazs and C. Yuan, *Phys. Rev.* **D56** (1997) 5558–5583, [hep-ph/9704258](#).
- [25] W. Placzek and S. Jadach, *Eur. Phys. J.* **C29** (2003) 325–339, [hep-ph/0302065](#).
- [26] W. Placzek, *PoS EPS-HEP2009* (2009) 340, [0911.0572](#).
- [27] A. Martin, W. Stirling, R. Thorne, and G. Watt, *Eur. Phys. J.* **C63** (2009) 189–285, [0901.0002](#).
- [28] A. Banfi, M. Dasgupta, S. Marzani, and L. Tomlinson, *JHEP* **01** (2012) 044, [1110.4009](#).
- [29] A. Banfi, M. Dasgupta, S. Marzani, and L. Tomlinson, *Phys. Lett.* **B715** (2012) 152, [1205.4760](#).
- [30] D0 Collaboration, V. M. Abazov *et al.*, *Phys. Rev. Lett.* **106** (2011) 122001, [1010.0262](#).
- [31] LHCb Collaboration, R. Aaij *et al.*, *JHEP* **02** (2013) 106, [1212.4620](#).
- [32] S. Alioli, P. Nason, C. Oleari, and E. Re, *JHEP* **1006** (2010) 043, [1002.2581](#).
- [33] T. Sjostrand, S. Mrenna, and P. Z. Skands, *JHEP* **0605** (2006) 026, [hep-ph/0603175](#).
- [34] T. K. O. Doan, *CERN-THESIS-2013-001*, *Mesure de la section efficace différentielle de production du boson Z se désintégrant en paires électron-positon, dans l'expérience ATLAS*, available from <https://cds.cern.ch/record/1503540/>.